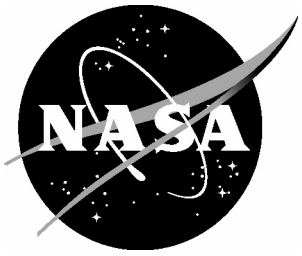
NASA/TM–20250008896



Multiple Mechanical Behaviors of Carbon Nanotube Fiber Reinforced Epoxy Composites

Jae-Woo Kim
Analytical Mechanics Associates, Hampton, Virginia

John M. Gardner, Godfrey Sauti, Benjamin D. Jensen, Russell A. Wincheski, Joseph G. Smith, Scott R. Zavada, Kristopher E. Wise, and Emilie J. Siochi
Langley Research Center, Hampton, Virginia

September 2025

NASA STI Program Report Series

Since its founding, NASA has been dedicated to the advancement of aeronautics and space science. The NASA scientific and technical information (STI) program plays a key part in helping NASA maintain this important role.

The NASA STI program operates under the auspices of the Agency Chief Information Officer. It collects, organizes, provides for archiving, and disseminates NASA's STI. The NASA STI program provides access to the NTRS Registered and its public interface, the NASA Technical Reports Server, thus providing one of the largest collections of aeronautical and space science STI in the world. Results are published in both non-NASA channels and by NASA in the NASA STI Report Series, which includes the following report types:

- TECHNICAL PUBLICATION. Reports of completed research or a major significant phase of research that present the results of NASA Programs and include extensive data or theoretical analysis. Includes compilations of significant scientific and technical data and information deemed to be of continuing reference value. NASA counterpart of peer-reviewed formal professional papers but has less stringent limitations on manuscript length and extent of graphic presentations.

- TECHNICAL MEMORANDUM. Scientific and technical findings that are preliminary or of specialized interest, e.g., quick release reports, working papers, and bibliographies that contain minimal annotation. Does not contain extensive analysis.

- CONTRACTOR REPORT. Scientific and technical findings by NASA-sponsored contractors and grantees.

- CONFERENCE PUBLICATION. Collected papers from scientific and technical conferences, symposia, seminars, or other meetings sponsored or co-sponsored by NASA.

- SPECIAL PUBLICATION. Scientific, technical, or historical information from NASA programs, projects, and missions, often concerned with subjects having substantial public interest.

- TECHNICAL TRANSLATION. English-language translations of foreign scientific and technical material pertinent to NASA's mission.

Specialized services also include organizing and publishing research results, distributing specialized research announcements and feeds, providing information desk and personal search support, and enabling data exchange services.

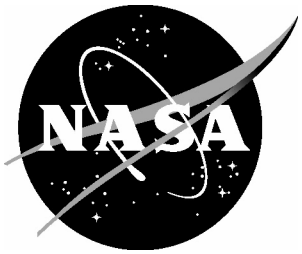
For more information about the NASA STI program, see the following:

- Access the NASA STI program home page at http://www.sti.nasa.gov

- Help desk contact information:

https://www.sti.nasa.gov/sti-contact-form/
and select the "General" help request type.

NASA/TM–20250008896



Multiple Mechanical Behaviors of Carbon Nanotube Fiber Reinforced Epoxy Composites

Jae-Woo Kim
Analytical Mechanics Associates, Hampton, Virginia

John M. Gardner, Godfrey Sauti, Benjamin D. Jensen, Russell A. Wincheski, Joseph G. Smith, Scott R. Zavada, Kristopher E. Wise, and Emilie J. Siochi
Langley Research Center, Hampton, Virginia

National Aeronautics and
Space Administration

Langley Research Center
Hampton, Virginia 23681-2199

September 2025

The use of trademarks or names of manufacturers in this report is for accurate reporting and does not constitute an official endorsement, either expressed or implied, of such products or manufacturers by the National Aeronautics and Space Administration.

ABSTRACT

Carbon nanotube fibers have been considered as a reinforcement in lightweight composites. Despite recent improvements in carbon nanotube fiber production rates and tenacities, mechanical properties of carbon nanotube fiber composites and corresponding processing methods have been limited to tensile property studies. Consideration of carbon nanotube fiber reinforced polymer composites in structural applications requires a broad characterization of their performance under a variety of loading conditions. To that end, short beam strength, axial flexure, transverse flexure, compression, and tension tests are conducted on carbon nanotube fiber reinforced epoxy composites. For each test, composites made from three different formats of carbon nanotube fiber reinforcement with a high weight (or volume) percentage of reinforcement up to 70 wt.% (68 vol.%) are compared. Each composite shows unique mechanical behaviors dependent on the loading environment and carbon nanotube fiber format. This dataset may serve as guidance for the further improvement of carbon nanotube fiber reinforced composites' mechanical properties and processing optimization.

KEYWORDS. Carbon nanotube fiber, composite fiber, epoxy, multiple mechanical properties.

1. Introduction

The unique properties of carbon nanotubes (CNTs) applicable to mechanical, thermal, and electrical applications have driven a variety of advancements and given rise to the availability of various CNT product formats that include powders, fibers, and sheets [1-5]. Nevertheless, their practical applications in lightweight structures have been limited. One reason for this is the lack

of panel-level data on the mechanical properties of composites incorporating CNT formats, especially continuous CNT fibers (CNTFs).

Advancements in CNTF manufacturing [6-9] have enabled the study of coupon-scale composites with continuous CNTF reinforcement focused on tension-driven structural applications [10]. The mechanical characterization of CNTF reinforced polymer composites has consisted primarily of tensile strength and modulus of thin films that were a few hundred micrometers thick with gauge lengths of less than 20 mm [11-17]. In earlier work, unidirectional CNTF/bismaleimide (BMI) composites were reported with specific tensile strength up to 2 GPa/(g/cm^3) [15] and specific modulus up to 225 GPa/(g/cm^3) [18]. Limited characterization of other mechanical properties such as short beam strength (SBS), compression, fracture toughness, and flexure has been conducted [11,15,19-20].

Unidirectional CNTF composites had much lower mechanical properties than state-of-the-art composites like carbon fiber (CF) reinforced polymer composites when loaded in other directions, including SBS (9.1 MPa) [11], compression strength (130 MPa), compression stiffness (10.0 GPa) [19], flexural strength (514 MPa), and flexural modulus (47.3 GPa) [20]. This has been attributed to both poor interfacial shear strength (IFSS, < 5 MPa) within the CNTF [21] and relatively low (or unoptimized) volume fraction (18 – 39 vol.%) of CNTFs in the composites.

Recent improvements in tenacity and interfacial shear behaviors of the CNTF have been reported with a polymer infiltration process that occurs while the fibers are being produced [14,22-23]. This process resolved the dry-core shear failure of the fiber observed in CNTF composites. For example, Kim *et al.* developed a method for producing an intermediate material for composite fabrication through stretching and aligning CNT roving where epoxy resin and

ionic liquid (IL) were incorporated during the processing, resulting in a CNT/epoxy/IL prepreg [22]. This method afforded epoxy infiltration deep into the hierarchical CNT fiber microstructure that improved the apparent interfacial shear strength (≥ 17.5 MPa) of the resultant material. High CNT alignment was achieved during the stretching process resulting in enhanced fiber tenacity of up to 1.7 N/tex and specific modulus up to 99 GPa/(g/cm^3) with linear densities in the 6 to 9 tex range. Another important aspect of this work is that the processed CNT/epoxy/IL prepreg can be stored either at ambient conditions (up to 60 days with 3.5 wt.% IL) or in a freezer for later use in composite part fabrication. However, the mechanical behavior of composites made with this material has not been comprehensively investigated.

An engineering-level systems analysis of the deployment and performance of CNTs in real applications is quite challenging but necessary before significant investment or adoption of CNTs can be realized [24]. Determining of a more extensive set of mechanical properties is vital for understanding where to focus improvements on the CNT material system and, in aerospace structural applications, for identifying specific components where CNTs could provide systems-level benefits.

Therefore, in this study, the mechanical behaviors of unidirectional CNTF reinforced epoxy composites are characterized and their failure modes described under multiple loading conditions including SBS, axial and transverse flexure, combined load compression, and tension. Composites are fabricated from three different CNTF formats: (1) loosely networked CNT roving, (2) highly densified and aligned CNTF (HD-CNTF), and (3) cured CNT/epoxy/IL composite fiber (CNT-CoF) prepared from CNT/epoxy/IL prepreg as described in previous work [22]. These three formats broadly cover the range of CNTF options that are currently available for composite part fabrication. This report focuses on providing mechanical properties along

with descriptions of failure modes for each loading condition and discusses the relationship between the mechanical behaviors of the CNTF composites and their micro-structure for each type of CNTF to aid in future material design for specific applications.

2. Experimental

The mechanical behavior of unidirectional composites made using three different types of CNTF were compared in this work. Multiple samples of each composite were fabricated under various composite processing conditions. The processing variables investigated included IL concentration, cure method such as autoclave or hot press, and various cure cycles. Each composite material was processed under slightly different processing conditions, in an iterative effort to maximize the mechanical properties with reasonable processibility. However, not all the mechanical behaviors and processibility of the sample in each condition are discussed in this work due to their complex relationship for each CNTF type used. A select subset, highlighting key findings from the investigation, is discussed instead. The samples that are discussed in this report were prepared as described in the sections that follow.

2.1. Materials

The room temperature ionic liquid 1-ethyl-3-methylimidazolium dicyanamide (EMIM-DCA, Sigma-Aldrich[1]), EPON™ 828 (Hexion Inc.) which is a bisphenol A/epichlorohydrin derived liquid epoxy resin, acetone (Fisher Scientific), and acetonitrile (ACN, Sigma-Aldrich) were used as-received.

[1] *Specific vendor and manufacturer names are explicitly mentioned only to accurately describe the test hardware. The use of vendor and manufacturer names does not imply an endorsement by the U.S. Government nor does it imply that the specified equipment is the best available.*

In this work, three different types of CNTF were used to fabricate unidirectional CNTF reinforced epoxy composite coupons including CNT roving, HD-CNTF, and CNT-CoF, whose processing is described in Reference 22. HD-CNTF and CNT roving used as-is for composite coupon fabrication and as a starting material for the processing of CNT-CoF were purchased from Nanocomp Technologies (Huntsman Corporation). The thin, tape-like, aerogel-spun CNT roving is a low-density fibrous CNT product harvested directly from the floating catalyst-chemical vapor deposition (FC-CVD) process [25]. CNT roving materials can be continuously produced from FC-CVD aerogel spinning and are currently available in lengths of several kilometers. The as-produced CNT roving materials used in this work were hundreds of microns wide and only tens of microns thick, giving them a tape-like cross-section. In contrast to other studies with low linear density CNTFs (< 1 tex) [26-27], the CNT roving materials, HD-CNTFs, and processed CNT-CoFs used in this work have a relatively higher linear density (9 - 12 tex). Physical properties of the used CNTFs are summarized in Table 1.

The CNT-CoF was prepared from a CNT/Epoxy/IL prepreg stretched to 40 %. About eight hundred meters of as-processed prepreg, required for each composite coupon, was wrapped in multiple layers on a 30.48 cm × 30.48 cm solid aluminum fixture using a custom-built winder. Visible separation was maintained between each prepreg strand in a layer. Each layer was in turn separated from the next by a porous release fabric (Airtech, Release Ease 234TFP) to prevent adhesion between the layers. The prepreg wrapped on the fixture was cured at 165°C for 2 hours and further post-cured at 200°C for 2 hours in an air oven, resulting in the processed CNT-CoFs. The resin and IL content in the cured CNT-CoF ranged between 16 and 20 wt.%.

2.2. CNTF reinforced epoxy composite processing

In the case of the CNT roving/epoxy composite, the part was fabricated by solvent-assisted infiltration of epoxy resin during direct winding of the CNT roving onto a solid stainless-steel fixture (~ 10 cm length). The roving was laid down in a brick-and-mortar (BAM) pattern (500 μm pitch and 60 mm wide). A mixed ACN solution that contained 4 wt.% EMIM-DCA in 20 g of EPON™ 828 mixed with an additional 80 g of ACN was applied layer-by-layer by a brush during the winding. The total CNT roving length and number of layers for the composite coupon were 1687 m and 59 layers, respectively. The winding process was performed using a modified desktop filament winder (X-winder®, 2-Axis) [15]. The as-wound sample was placed in a mold and cured in a hot press. The custom-designed mold setup for the press consisted of the wound part sandwiched between two plungers, top and bottom, with two pairs of blocks placed as side dams to prevent fiber spreading during the cure cycles (Supporting Information Figure S1a). The following cure cycle was used: full vacuum at room temperature was applied, the temperature increased to 130°C and held for 30 min, then a platen pressure of 1.38 MPa was applied, then the temperature increased to 165°C and held for 2 hours followed by a temperature ramp to 200°C and held for 2 hours and then cooled to room temperature. All temperature ramps were at a nominal rate of 2.78°C/min.

In the case of the HD-CNTF/epoxy composite, as-purchased HD-CNTF (Nanocomp, 2.16 N/tex tenacity and total length 805 m) was used to fabricate a composite part with 33 layers (250 μm pitch and 30 mm wide) by applying resin solution (10 wt.% EMIM-DCA in 10 g of EPON™ 828 mixed with additional 20 wt.% ACN) layer-by-layer by a brush during the winding process. The mold set-up and cure cycle were the same as that used for the CNT roving composite process except for the first hold temperature which was set at 110°C instead of 130°C. The

change in the first temperature hold was informed by results of rheological testing and observations from the CNT roving composite processing.

As-processed CNT-CoF (1.43 N/tex tenacity and total length 808 m) was used to fabricate a CNT-CoF/epoxy composite part with 33 layers (250 μm pitch and 30 mm wide) by applying resin solution (3 wt.% EMIM-DCA in 10 g of EPON™ 828 with no additional solvent) layer-by-layer by a brush during the winding process. The mold set-up and cure cycle were the same as the HD-CNTF composite process. It must be noted that optimization of composite processes for each CNTF composite is out-of-scope in this report which focused instead on the material properties following similar processing.

2.3. Specimen preparation and mechanical tests

Each cured composite part, shaped as a rectangular band with flat faces and rounded edges from the molding tool, was separated into two flat coupons by removing the curved edges using a low-speed diamond saw (Buehler, IsoMet®). The two coupons of each unidirectional composite were cut to make 6 mm wide × 70 mm long tension, compression, and axial flexure (AF) specimens. SBS and transverse flexure (TF) specimens were cut to dimensions that ensured that the width to thickness and length to thickness ratios were 2 and 6, respectively (Supporting Information Figure S1b-d). For example, the width and length of SBS and TF specimens were 3 mm and 9 mm, respectively, when the coupon thickness was 1.5 mm. Test specimens from the CNT roving and HD-CNTF composites were precisely cut using a precision waterjet cutter (Microwaterjet®, Meyer Tool Huntersville, LLC, dimensional tolerance of 0.01 mm). The CNT-CoF composite test specimens were precisely cut using a high-speed saw with a custom-designed diamond blade (Continental Diamond Tool).

Specimen thickness was measured using a digimatic indicator (Mitutoyo Corp., Model ID-F125E) read by a computer while length and width were measured using vernier calipers. The nominal densities of the specimens were determined by dividing the measured weight by the volume obtained from averaged lengths, widths, and thicknesses measured at multiple locations. Room temperature axial tensile and combined load compression (CLC) responses of the unidirectional CNTF composites were measured using an MTS Landmark servo-hydraulic test system equipped with a laser extensometer and a 25 kN load cell. The tests were run by pre-programmed test programs developed within the MTS TestSuite™ TW Elite package. For the axial tensile test, the gauge length and crosshead speed were 20 mm and 0.5 mm/min, respectively. The compression test was based on ASTM D6641/D6641M [Standard Test Method for Compressive Properties of Polymer Matrix Composite Materials Using a Combined Loading Compression (CLC) Test Fixture] with specimen dimensions proportionally scaled-down 50% to enable testing in a miniaturized CLC test fixture (Wyoming Test Fixture). The gauge length for axial strain measurement by the test frame actuator and crosshead speed were 6.5 mm and 1 mm/min, respectively. The precise strain under the compression load was measured by a laser extensometer with retroreflective tape applied on the test fixture.

SBS, AF, and TF of the samples were measured using an Instron 5844 load frame equipped with a 2 kN load cell and a miniaturized 3-point flexure test fixture (Wyoming Test Fixture). The AF test was based on ASTM D790 (Standard Test Methods for Flexural Properties of Unreinforced and Reinforced Plastics and Electrical Insulating Materials) maintaining a span/thickness ratio of 32 : 1. SBS and TF tests were based on ASTM D2344 (Standard Test Method for Short-Beam Strength of Polymer Matrix Composite Materials and Their Laminates)

with a scaled-down fixture and specimen dimensions suggested by the published literature [28]. The span to thickness ratio was maintained at 4 : 1 in both SBS and TF tests.

2.4. Calculation of resin content

The specimens prepared for the CLC tests were used to determine the resin content for each composite material type. Resin content in the CNTF composite samples was calculated based on the specimen mass, total CNTF length, average linear density of the CNTF used, the specimen dimensions, and number of layers in each specimen. The "resin content" in this report includes both the epoxy resin and IL in the composite.

2.5. X-ray computed tomography and microscopy

X-ray computed tomography (CT) data was taken using a Nikon Metrology system with a 2000 × 2000 pixel arrayed Perkin-Elmer 16-bit amorphous silicon digital detector with a maximum resolution of 5 μm. The three-dimensional reconstruction of the collected radiographs at each rotation angle (360° in 0.11° increments) produced tomographic data that can be viewed along any plane in the sample volume. X-ray CT was conducted before and in some cases after mechanical tests.

All specimen tests were monitored with a portable microscope (Aven, Mighty Scope V2 Digital Microscope, 200× max) to observe the failure mode under the applied load. Post-mortem fractography of the failed specimens was observed with an optical microscope (Leica DM8000 M) to provide further details on the failure mechanism.

3. Results and discussion

3.1. Physical properties of the starting materials and their composites

Physical properties for each type of CNTF and their respective composites are shown in Table 1. The thickness per layer varied depending on the CNTF format and processing conditions, especially the initial cure temperature and IL concentration. Generally, a higher concentration of IL in the system results in less consolidation at the initial cure temperature holding step, which occurs at either 110°C or 130°C before the application of cure pressure. This is due to the relatively short gelation time (~ 26.5 min with 3 wt.% IL versus ~ 6.5 min with 10 wt.% IL both at 130°C, Supporting Information Figure S2) and down shifting of the exothermic temperature with an increase of IL concentration [29].

As expected, the resin content in each CNTF composite differed the most based on the CNTF format. The CNT roving composite had the highest resin content (60.4 wt.%) as the loosely connected networks of CNTs give rise to a high volume of internal spaces which are accessible to and can be occupied by the epoxy and IL. On the other hand, the HD-CNTF is a solid fiber without accessible voids. Therefore, the applied resin mostly resides outside the fiber, resulting in a relatively lower resin content (27.7 wt.%). In the case of the CNT-CoF/epoxy composite, the CNT-CoF itself usually contains 26 wt.% of resin and IL. Therefore, the overall resin content in the CNT-CoF composites, which is the sum of the resin inside and outside the fiber, increased compared to that of the HD-CNTF composites. It is noted that the thickness per layer of the CNT-CoF composite decreased even with epoxy infiltrated inside of the CNT-CoF structure (43.7 μm vs. 48.2 μm in the HD-CNTF composite) due to the different cure cycles, especially the first cure temperature and IL concentration in the system.

Mechanical properties of the neat epoxy resin cured with various IL concentrations were measured and are summarized in Table S1 (Supporting Information). A system with higher IL concentration (10 wt.% IL) had a higher tensile strength and toughness but showed similar Young's modulus than those from the materials made with lower IL concentrations (3, 5, and 7 wt.%). This suggests that the IL incorporated in the epoxy system can act as a toughener, which agrees with the literature [30]. However, the effects of IL concentration on the mechanical properties of the composite system are relatively minimal compared to other factors such as CNTF format, cure cycle, and other processing conditions, especially for fiber dominated properties (Supporting Information Table S2 – 3, 5, and 10 wt.% CNT-CoF composite properties). A study of various CNT-CoF composites fabricated with varying IL concentrations in the system did not show recognizable differences in the mechanical properties measured under the various loading conditions. Therefore, in this report, only the mechanical behaviors of three specific CNTF reinforced epoxy composites made with each CNTF format are discussed.

3.2. Short beam strength (SBS) properties of CNTF composites

The SBS test was used to help understand the material behaviors, especially the interface between the CNTF and the matrix. It is noted that the CNTF composites studied do not have clear interlaminar layers where typical failure of carbon fiber reinforced polymer composites would be expected to occur. Only qualitative conclusions were drawn from the small-scale SBS tests of the CNTF composites due to the expected plasticity prior to ultimate failure, which is a typical observation in similar tests [28]. SBS properties of CNTF reinforced epoxy composites, measured using the test configuration recommended in Reference 28, are summarized in Table 2. As expected from previous single fiber pull-out tests and other studies [21,31-32], the HD-CNTF

composite showed the lowest SBS value (14.0 MPa). This can be attributed to poor interfacial shear strength within the dry HD-CNTF core, as opposed to the interface between the surface of the HD-CNTF and resin. The HD-CNTF composite experienced multiple delamination failures between the layers and inelastic deformation, after passing the elastic deformation point, because the composite did not have distinct interlaminar layers as shown in Figures 1a (red curve) and 1c. These multiple failures are not clear in the cross-sectional views at maximum load (Figure 1c) and upon unloading at the conclusion of the test (Figure 1c inset). However, their effects are visible in the SBS stress vs. displacement curve where there were multiple and continuous stress drops starting right after the maximum load (Figure 1a inset) and even after a big load drop at ~2.5 mm displacement. Among the CNTF composites tested, the HD-CNTF composite contained the least amount of resin and that may contribute to the multiple delamination failures.

Increased resin content in the composite system and CNTF format changed the failure mode under SBS load. The CNT roving composite showed an increase of more than 2 times in SBS (34.3 MPa) with a single delamination failure and without visible inelastic deformation [Figures 1a (black curve) and 1b (yellow arrow)]. In the case of the CNT-CoF composite, the SBS failure behavior is a mix of the behaviors of the two other composite types. Elastic behavior of both the HD-CNTF and CNT-CoF composites is nearly identical likely due to the similarity in the fiber reinforcement behavior. Both fibers have densified and aligned CNTs with similar tenacity and modulus. The increased SBS (40.3 MPa) of the CNT-CoF composite is attributed to the improvement of both intra- and inter-fiber interfacial shear properties by the infiltrated resin. However, the CNT-CoF composite exhibited multiple delamination failures with visible inelastic deformation [Figure 1a (blue curve) and 1d]. The multiple delamination failures were clearly observed under the optical microscope (OM) after the test as shown in Figure 1e. The post-

mortem OM image is a cross-sectional view taken edge-on and showed the typical failure behaviors of the layered structure. Interestingly, each failure starts at one side of the specimen and then propagates toward the other side with some undulated deflections or branching to other layers. The cracks mostly stop within the specimen before reaching the opposing edge. Multiple delamination failures of the CNT-CoF composite were observed at highly deformed and buckled locations as shown in Figure 1f. This occurred due to severe plastic deformation under high strain mostly close to the loading roller and support rollers. The deformations, kinks, and delamination were observed both within and between layers. Each layer thickness of the CNTF-CoF composite, including fiber and resin, was 43.7 μm (Table 1). The multiple delaminations that were observed had thickness of 10 to 20 μm based on the OM observation (Figure 1f). Therefore, the delamination also occurred within the single layer. This is somewhat similar to what was observed for the cured CNT-CoFs under tensile load, where longitudinal breakages in multiple locations were observed [22]. The inelastic deformation is not considered an acceptable SBS test failure mode due to severe plastic deformation instead of interlaminar shear failure (ASTM D2344). However, the test is instructive in understanding the behavior of the material.

3.3. Axial flexure (AF) properties of CNTF composites

For the AF test, the support span-to-thickness ratio was 32:1 to make sure that the failure was either shear delamination at the outer surface of the specimen on the tension side or local buckling at the inner surface on the compression side. The flexural strength, modulus, and strain were calculated based on beam theory as specified in ASTM D790. Representative flexural stress-strain curves of the CNTF composites are shown in Figure 2a. The related OM images and video frames captured at the final stage before release of the applied load are shown in Figures

2b-2d. Each CNTF composite had a distinctive bending behavior depending on the type of the CNTF used. The CNT roving composite had both multiple shear delaminations at the outer layers of the specimen in the tension direction and local buckling along with multiple shear delaminations on the inner compression side (Figure 2b). The flexural strength (214.6 MPa) and tangent modulus (27.7 GPa) of the CNT roving composite was relatively low because the CNT roving is not a highly stretched and densified format and is stretchable under both tensile and compressive forces even in the composite form.

When composites were made with stiffer fiber reinforcements, the tangent modulus increased mostly due to the effect of the fiber characteristics such as CNT alignment in the fiber. The modulus increase was particularly pronounced at high mass fractions of the fiber in the composite. The HD-CNTF composite with a 72.3 wt.% fiber loading had increases in both strength (459.9 MPa) and tangent modulus (116.2 GPa). However, the material prematurely and catastrophically failed by multiple shear delaminations parallel to the fiber axis without visible local buckling (Figure 2c). This is mostly due to the lack of resin and poor interfacial shear giving a maximum strain at failure of only 0.56 %. An earlier study showed flexural strength, tangent modulus, and maximum strain of 514 MPa, 47.3 GPa, and 4.5 %, respectively, for thin CNTF composites with 30 vol.% CNT fiber (1.16 N/tex tensile tenacity and 0.03 tex linear density) [20].

The CNT-CoF is a highly densified reinforcement format with resin infiltrated inside the fiber and CNT alignment that is intermediate between that of the CNT roving and HD-CNTF. It is therefore expected to have combined characteristics of both the HD-CNTF and the resin-infiltrated CNT roving. The early part of the flexural stress-strain curve followed the same trend as the HD-CNTF composite due to the similar characteristics of the fiber formats. The strain at

peak load for the stretched and aligned forms of CNTF composites was 0.56 % with the HD-CNTF and 0.66 % with the CNT-CoF. However, the CNT-CoF composite showed severe buckling at multiple locations with multiple delaminations occurring along with buckled lines (Figure 2d). This continuously dissipated the load locally and made the composite much tougher. The flexural strength and tangent modulus of the CNT-CoF composite were 484.0 MPa and 137.5 GPa, respectively, an improvement most likely arising from the incorporation of resin within the fiber. Local shear delamination failure inside the specimen was not observed likely because of the simultaneous improvement to the interfacial shear strength and tensile strength of the CNT-CoF composite. Interestingly, none of the CNTF composites studied showed tensile failure within the measured strain range.

3.4. Transverse flexure (TF) properties of CNTF composites

In contrast to SBS and AF, TF strength and failure modes of the CNTF composites differed dramatically depending on CNTF format. TF strength and tangent modulus of the CNT roving composite were 101.2 MPa and 3.2 GPa, respectively, the highest among the CNTF composites studied. These high values are due to the resin penetrating inside the loosely connected CNT roving networks and the hierarchical microstructure including BAM layup. Cracks deflected in multiple directions resulting in a long travel path with “shark teeth” traces, which is in good agreement with the literature [33-35]. The crack deflection resulted in a material that is much stronger and tougher under the TF load, which is in good agreement with the results obtained under the transverse tensile load in a previous study [15].

Even though the HD-CNTF composite also has a BAM structure, the cracks propagated through the weak dry section within the HD-CNTFs rather than at the HD-CNTF-resin interface.

This resulted in failure traces superficially like those observed for the CNT roving composite but weaker TF strength. As with the tensile strength of HD-CNTF composite [15], TF strength (21.1 MPa) and tangent modulus (0.8 GPa) remained low, a result of poor load transfer within the HD-CNTF. The specimen failed gradually under the TF load with visible pull-out of dry CNT bundles at the failure cracks (Figure 3c). In addition, the HD-CNTF composite contained micro-size voids located between the CNTFs, which further contributed to the poor shear and TF properties as shown in Figure 3e. Removing micro-voids (dark areas in Figure 3e) from the HD-CNTFs composites is very challenging, especially at normal composite cure pressures (~1.38 MPa) or even in the hot press while applying extreme pressure (~300 MPa) after the winding step [18].

The CNT-CoF composites contain a relatively low amount of micro-voids (~2 %) (Figures 3f-3g), owing to the improved wettability between the composite fibers and the additional resin applied during the filament winding. This resulted in a compact and homogeneous internal structure throughout the sample. There were still a significant number of resin rich regions located mostly at the CNT-CoF ends (between the “bricks” in the BAM structure) (Figure 3g and inset). The dark areas in the images are resin rich, the “mortar” in the BAM structure and not voids, which was confirmed by x-ray CT scan (Figure 3f). Due to the resin infiltrated inside the fibers, TF strength (45.9 MPa) and modulus (1.2 GPa) of the CNT-CoF composite improved compared to those from the HD-CNTF composite but were not better than those from the CNT roving composites. Interestingly, the crack propagation in the CNT-CoF composite did not show similar patterns to those observed in the HD-CNTF and CNT roving composites as shown in Figures 3d and 3f. The crack propagates through the fibers instead of following the interface between the composite fiber and the resin (mortar or resin) in the specimen. Even though resin is

incorporated into the CNT-CoFs, the CNTs (or CNT bundles) in the fiber are highly stretched and aligned along the fiber axis direction. This results in the relatively lower tensile strength in the transverse direction compared to composites with randomly aligned CNT networks [35]. Similarly, the CNT-CoF has the weakest strength in the longitudinal direction along the aligned CNT-CoFs that is in good agreement with multiple breakages of sub-structures failed along the fiber axis under the tensile load [22]. The CNT-CoF composite sample appears to have homogeneous mechanical properties causing the relatively smooth crack propagation parallel to the loading direction as shown in Figures 3d and 3f. It is noted that the effects of the cross-sectional aspect ratio of the CNT-CoF, resin thickness between the fibers, and internal structures such as BAM for the mechanical behaviors are not discussed in this work. For example, the CNT roving composite has a cross-sectional aspect ratio of about 10.9, calculated based on the placement pitch and the thickness per layer while the HD-CNTF and CNT-CoF composites have 6.6 and 5.7 aspect ratio, respectively.

3.5 Compression properties of CNTF composites

Compressive strength and modulus of unidirectional fiber reinforced polymer composites are influenced by various factors including the microstructure of the reinforcement, internal structure design (such as BAM), interfacial properties, and process induced defects such as voids, dry spots, and fiber misalignment along with manufacturing methods [36-37]. Mostly, voids in the composites act as geometrical stress concentrators leading to micro-crack development in the polymer matrix and premature fiber-matrix debonding which results in the kink band failure mode. Fiber misalignment in the composites also contributes to the kink band failure mode. In addition, compressive strength and modulus are especially sensitive to overall void content in

unidirectional composites. As-fabricated CNTF composites were tested under combined loading compression to minimize the shear stress peaks at the specimen tip resulting in a uniform stress distribution along the gauge length. It was difficult to classify the failure mode under the compressive load with the non-optimized CNTF composites. Therefore, the general observations of the material response and failure are shared as an example for each CNTF composite.

The CNT roving composite first showed vertical delamination between layers as a premature interfacial failure in the longitudinal direction (Figure 4b, yellow arrow in the second image). This was followed by a kink band failure, which resulted from deformation of the fibers. Failure then proceeded via micro-buckling and rotation of the fiber and finally by local fiber kinking under further compressive strain (Figure 4b). It clearly appears that the interfacial crack growth precedes the kink band formation and even micro-buckling process which agrees with literature [36]. The CNT roving reinforcement with polymer resin infiltration could tolerate large shear deformations in the through-thickness direction. However, tensile breaks within the kink band boundaries were often observed at multiple locations during the post-mortem fractographic analysis (Figure 4c, red arrows). Due to the characteristics of the CNT roving and filament winding process, the CNT roving composite possibly contains misaligned fibers and regions with fiber waviness as internal defects, which would cause the creation of shear planes and thus the occurrence of significant shear deformation in the through-thickness kink band failures.

Generally, mixed failure modes including multiple longitudinal splitting of layers and followed by delamination buckling and wedge splitting (Figures 4d and 4e) appear in the HD-CNTF composite due to poor shear properties of the composite as shown in the SBS results (Figure 1a and Table 2). The existence of voids from the composite processing (Figure 3e) and poor IFSS caused by the dry core within the fiber and confirmed in single fiber pull-out tests [21],

contributed to the low compressive performance. Nevertheless, among the three composite formats assessed, the compressive strength of the HD-CNTF composite was the highest at 231.3 MPa. This is most likely due to the high alignment of CNTs in the fiber during the manufacturing process of the HD-CNTF (> 60 % stretch).

The compressive strength (201.6 MPa) of the CNT-CoF composite is not improved relative to the HD-CNTF composite even though the interfacial shear properties improved through pre-infiltration of resin. The compressive modulus of the CNT-CoF composite (13.1 GPa) was comparable to the HD-CNTF composite when accounting for the scatter. More studies are required to better understand the relationships between compressive strength, composite processing conditions, and reinforcement types for CNTF composites. As shown in Supporting Information Table S2, compressive strength of the CNT-CoF composites does not linearly vary with the IL concentration used in processing but rather rises then drops. The compressive strength of the composite fabricated with 5 wt.% IL showed the highest value (233.7 MPa), while the composite with 10 wt.% IL provided the lowest value (196.2 MPa) even though the strength of the neat resin with 10 wt.% IL was the highest (Supporting Information Table S1). The modulus of the CNT-CoF composites does appear not to be as sensitive to the IL concentration with all the values lying within the scatter. Interestingly, the compressive failure of the CNT-CoF composite showed mixed modes including shear failures in multiple directions.

3.6 Tension properties of CNTF composites

The axial tensile properties of the CNT-CoF composite were measured and compared with values for the CNT roving and HD-CNTF composites from previously reported data [15]. The specific stress-strain curves of the CNTF composites are presented in Figure 5. The tensile

strengths of the unidirectional fiber reinforced composites depend on the reinforcement fiber properties. Property decreases from fiber to composite were observed when highly stretched CNTFs such as HD-CNTF and CNT-CoF were used; conversely, the composite made from the loosely networked CNT roving yielded property improvement. The specific strength and modulus of the CNT roving composite were improved significantly through the fabrication process that creates multi-scale hierarchical structures, which can improve both nano-scale and micro-scale load transfer within the fiber and between the fiber and surrounding polymer matrix as described in the reference 15. However, the HD-CNTF composite showed some knock-down of the specific strength due to premature failure of the fibers from poor load sharing between neighboring fibers [15]. The measured specific strength and modulus of the CNT-CoF composite were 1.09 GPa/(g/cm^3) and 64.7 GPa/(g/cm^3), which are 76% and 115% of the starting fiber values, respectively. The CNT-CoF composite showed multiple premature longitudinal failures of the individual fibers and fiber bundles at high tensile strain (~>3% strain) as shown in Figure 5. This premature fiber failure originates from the fiber failure characteristics when they have low resin content [22] and the weak shear property between the fiber and the polymer matrix.

3.7 Comparison of multiple mechanical properties of CNTF composites

Figure 6 presents radar charts of the mechanical properties discussed in Table 2 (as specific values, normalized by density) for a side-by-side comparison to give a better understanding of the relationship between the CNTF reinforcement and each mechanical property. Apples-to-apples comparison of these values is quite difficult with non-optimized composite systems. However, it is valuable to provide baseline data and general observations of the behaviors of

multiple mechanical responses of the composites fabricated with the different types of CNTF to define the bounds of the material design space.

Each CNTF composite has its own advantages and disadvantages with respect to mechanical properties under various loading conditions. Generally, CNT alignment within the fiber is one of the important factors for specific tensile strength (STS) and modulus (STM), specific axial flexural strength (SAFS) and modulus (SAFM), and specific compressive strength (SCS) and modulus (SCM). Pre-infiltration of resin into the CNTF to improve interfacial shear properties of intra- and inter-fibers is another important factor for shear related mechanical properties such as specific short beam shear strength (SSBSS), specific transverse flexural strength (STFS) and modulus (STFM). It is not clear what role the internal structure of the composite, like BAM structure, plays in determining each mechanical property except STFS and SSBSS. In this work, the influence of resin content on the CNTF composite is not discussed further because each CNTF system has its own optimum resin content for each mechanical property. In addition, the IL concentration in the system and cure conditions including cure temperature and time affect the final composite properties, especially some specific mechanical properties such as SCS (Supporting Information Table S2). There is still need for more thorough studies to address the impacts of material selection and processing parameters on the resulting composite properties.

5. Summary

Mechanical properties of unidirectional CNTF reinforced epoxy composites have been explored under multiple loading methods. Three different CNTF formats were compared as a reinforcement for polymer composite: CNT roving, HD-CNTF, and CNT-CoF. The mechanical

behaviors and failure mode of the composites varied depending on the type of CNTF used and the loading method.

The key findings resulting from this work include:

- The CNT roving can be infiltrated with resin during the wet winding process due to the loose open CNT network. Introducing polymer within the CNT roving reinforcement mitigates the dry-core shear failure seen in HD-CNTFs. The CNT roving reinforcement had the lowest alignment of the three formats tested, resulting in mechanical properties that are less anisotropic than the stretched and aligned formats. The improvement in interfacial shear resulted in an improved SBS (34.3 MPa) relative to the HD-CNTF composites. However, the CNT roving is not a highly stretched format, resulting in relatively lower tensile (1.12 GPa) [15], CLC (184.3 MPa) and AF (214.6 MPa) strengths, but higher TF strength (101.2 MPa) than the HD-CNTF and CNT-CoF composites.
- The HD-CNTF composite has densified and aligned CNTs within the fiber. However, resin cannot be readily infiltrated inside the fiber, leading to weak shear properties due to the poor load transfer within the fiber. This resulted in composites with high tensile (3.03 GPa) [15] and AF (459.9 MPa) strengths but poor SBS (14.0 MPa) and TF strength (21.1 MPa). Failure occurred within the dry core of the HD-CNTF in the composite.
- The CNT-CoF is pre-infiltrated with resin during the stretching process, which results in some CNT alignment and resin incorporation inside the fiber. This improves both the inter- and intra-fiber shear strength in the composite. The resin infiltration prior to composite processing and stretching improves overall mechanical properties of the

composite under the various loading methods relative to the CNT roving composite except under TF loading. As previously discussed, the CNT-CoF composite is expected to have more isotropic distribution of the CNTs. Therefore, the CNT-CoF composite behavior under TF load still requires more investigation including the cross-sectional aspect ratio effect in the BAM structure and resin content in the individual fiber.

- Isolation of the CNTF properties that influence the compressive behaviors of the composites is challenging. The failure modes of the CNTF composites under compressive load changed depending on the type of CNTF and processing conditions.

Overall, the incorporation of specific CNTF types in the composite is the main driving factor for the observed mechanical property and the failure mode changes. Understanding the mechanical behaviors of the various CNTF formats prior to their use in an application is important for the design of new CNT composite materials for targeted applications.

The properties of CNT composites have improved in recent years alongside increasing material availability, which has enabled the exploration of new processing routes, testing of larger coupons, and the characterization of multiple mechanical properties. However, the current mechanical properties do not make CNT composites an obvious drop-in replacement of highly optimized carbon fiber composites. For practical applications, it is expected that CNTs and their composites will expand the design space available to designers with unique challenges in addition to carbon fibers, polyparaphenylene benzobisoxazole (Zylon®), ultra-high-molecular-weight polyethylene (Dyneema®), liquid crystalline aromatic polyester (Vectran®), para aramid (Kevlar®), meta aramid (Nomex®), and other high performance fibers depending on the specific requirements of the component and the various advantages of the material options.

ACKNOWLEDGMENT

This work was funded through the Super-lightweight Aerospace Composites project under the NASA Space Technology Mission Directorate Game Changing Development Program. The authors would like to acknowledge Nanocomp Technologies (Huntsman Corporation) for insightful discussions and Mr. Sean Britton and Mr. Wilfredo Flores for their dedication on the composite processing.

REFERENCES

[1] Gohardani O, Elola MC, Elizetxea C. Potential and prospective implementation of carbon nanotubes on next generation aircraft and space vehicles: A review of current and expected applications in aerospace sciences. Prog Aerosp Sci 2014;70:42-68.

[2] Kinloch IA, Surh J, Lou J, Young RJ, Ajayan PM. Composites with carbon nanotubes and graphene: An outlook. Science 2018;362:547-553.

[3] Zhang S, Ma Y, Suresh L, Hao A, Bick M, Tan SC, Chen J. Carbon nanotube reinforced strong carbon matrix composites. ACS Nano 2020;14:9282-9319.

[4] Natarajan B. Processing-structure-mechanical property relationships in direct formed carbon nanotube articles and their composites: A review. Compos Sci Technol 2022;225:109501.

[5] Pendashteh A, Mikhalchan A, Varela TB, Vilatela J. Opportunities for nanomaterials in more sustainable aviation. Discover Nano 2024; 19:208.

[6] Smail F, Boies A, Windle A. Direct spinning of CNT fibres: Past, present, and future scale up. Carbon 2019;152:218-232.

[7] Lee J, Lee D-M, Jung Y, Park J, Lee HS, Kim Y-K, Park CR, Jeong HS, Kim SM. Direct spinning and densification method for high-performance carbon nanotube fiber. Nat Commun 2019;10:2962.

[8] Taylor LW, Dewey OS, Headrick RJ, Komatsu N, Peraca NM, Wehmeyer G, Kono J, Pasquali M. Improved properties, increased production, and the path to broad adoption of carbon nanotube fibers. Carbon 2021;171:689-694.

[9] Cho YS, Lee JW, Kim J, Jung Y, Yang SJ, Park CR. Superstrong carbon nanotube yarns by developing multiscale bundle structures on the direct spin-line without post-treatment. Adv Sci 2023;10:2204250.

[10] Kim J-W, Sauti G, Cano RJ, Wincheski RA, Ratcliffe JG, Czabaj M, Gardner NW, Siochi EJ. Assessment of carbon nanotube yarns as reinforcement for composite overwrapped pressure vessels. Compos A 2016;84:256-265.

[11] Kim J-W, Sauti G, Wincheski RA, Cano RJ, Jensen BD, Smith JG, Wise KE, Siochi EJ. Unidirectional carbon nanotube yarn/polymer composites, NASA TM 2018;220081.

[12] Mikhalchan A, Vilatela JJ. A perspective on high-performance CNT fibres for structural composites. Carbon 2019;150:191-215.

[13] Lin W, Shi QQ, Chen H, Wang JN. Mechanical properties of carbon nanotube fibers reinforced epoxy resin composite films prepared by wet winding. Carbon 2019;153:308-314.

[14] Shi QQ, Zhan H, Mo RW, Wang JN. High-strength and toughness carbon nanotube fiber/resin composites by controllable wet-stretching and stepped pressing. Carbon 2022;189:1-9.

[15] Kim J-W, Gardner JM, Sauti G, Wincheski RA, Jensen BD, Wise KE, Siochi EJ. Multi-scale hierarchical carbon nanotube fiber reinforced composites towards enhancement of axial/transverse strength and fracture toughness, Compos A 2023;167:107449.

[16] Park JG, Evers C, Jolowsky C, Vondrasek B, Thagard K, Czabaj M, Ku B, Wang Y, Dumitrica T, Odegard G, Laing Z. Gamma-ray irradiation to achieve high tensile performance of unidirectional CNT yarn laminates. Carbon 2024;216:118530.

[17] Vondrasek B, Evers C, Jolowsky C, Odegard GM, Liang Z, Czabaj M. Characterization of multidirectional carbon-nanotube-yarn/bismaleimide laminates under tensile loading. Compos B 2024;280:111465.

[18] Evers C, Kurilich M, Park JG, Jolowsky C, Thagard K, Liang Z. Multifunctional properties of carbon nanotube yarn/aerogel laminate composites. Compos B 2024;280:111495.

[19] Mora RJ, Vilatela JJ, Windle AH. Properties of composites of carbon nanotube fibres. Compos Sci Technol 2009;69:1558-1563.

[20] Mikhalchan A, Gspann T, Windle A. Aligned carbon nanotube-epoxy composites: the effect of nanotube organization on strength, stiffness, and toughness. J Mater Sci 2016;51:10005-10025.

[21] Kim J-W, Sauti G, Jensen BD, Smith JG, Wise KE, Wincheski RA, Cano RJ, Siochi EJ. Modifying carbon nanotube fibers: A study relating apparent interfacial shear strength and failure mode. Carbon 2021;73:857-869.

[22] Kim J-W, Gardner JM, Sauti G, Jensen BD, Wise KE, Wincheski RA, Smith JG, Zavada SR, Siochi EJ. Fabrication of carbon nanotube epoxy prepreg towards lightweight structural composites, Compos B 2024;275:111329.

[23] Durso MN, Sawyer WJ, John Hart A. Versatile fabrication of carbon nanotube yarn composites by in-situ interfacial polymerization of polyetherimide. Compos B 2024;287:111770.

[24] Samareh JA, Siochi EJ. Systems analysis of carbon nanotubes: opportunities and challenges for space applications. Nanotechnol 2017;28:372001.

[25] Durso MN, Sawyer WJ, John Hart A. Physical properties of industrially produced carbon nanotube yarns for use in structural nanocomposites. Compos B 2024;287:111821.

[26] Mikhalchan A, Gspann T, Windle A. Aligned carbon nanotube-epoxy composites: the effect of nanotube organization on strength, stiffness, and toughness. J Mater Sci 2016;51:10005-10025.

[27] Qiu J, Torrones T, Vilatela JJ, Vickers ME, Elliott JA, Windle AH. Liquid infiltration into carbon nanotube fibers: Effect on structure and electrical properties. ACS Nano 2013;7:8412-8422.

[28] Allott NR, Czabaj MW. Characterization of the interlaminar shear strength of IM7/8552 using small-scale short beam shear tests, Compos A 2021;142:106200.

[29] Aflal M, Rahmathullah M, Jeyarajasingam A, Merritt B, VanLandingham M, McKnight SH, Palmese GR. Room temperature ionic liquids as thermally latent initiators for polymerization of epoxy resins. Macromol 2009;42:3219-3221.

[30] Jeyarajasingam A. Imidazolium dicyanamide based room temperature ionic liquids as latent curing agents for epoxy systems. PhD dissertation of Drexel University, June 2012.

[31] De Leon A, Tank M, Sweat R. A scalable fiber bundle pullout manufacturing method for data-driven interfacial shear strength measurements of micro and nanomaterials. Compos Sci Technol 2022;222:109375.

[32] Bourdeau J, Mintz KJ, Jony B, Kirmani MH, Gupta K, Kumar S. Improvement of apparent IFSS and specific modulus of CNT yarns. Compos B 2024;284:111683.

[33] Rabiei R, Bekah S, Barthelat F. Failure mode transition in nacre and bone-like materials. Acta Biomater 2010;6:4081-4089.

[34] Narducci F, Pinho ST. Interaction between nacre-like CFRP mesolayers and long-fiber interlayers. Compos Struct 2018;200:921-928.

[35] Jensen BD, Kim J-W., Sauti G., Wise KE, Dong L, Wadley HNG., Park JG, Liang R, Siochi EJ. Toward ultralight high strength structural materials via collapsed carbon nanotube bonding. Carbon 2020;156: 538-548.

[36] Opelt CV, Cândido GM, Rezende MC. Compressive failure of fiber reinforced polymer composites – A fractographic study of the compression failure modes. Mater Today Commun 2018;15:218-227.

[37] Nunna S, Ravindran AR, Mroszczok J, Creighton C, Varley RJ. A review of the structure factors which control compression in carbon fibres and their composites. Compos Struc 2023;303:116293.

Table 1. Physical properties of CNTF reinforcements and their polymer composites.

	Uni CNT roving/epoxy composite	Uni HD-CNTF/epoxy composite	Uni CNT-CoF/epoxy composite
CNTF reinforcement			
Average linear density (g/km or tex)	10.517	10.866	11.339
Average tenacity [N/tex or GPa/(g/cm^3)]	0.48	2.16	1.43
Average specific modulus (N/tex)	12.8	84.3	56.1
CNTF composites			
Number of layers	59	33	33
Thickness (mm)	2.711 ± 0.129	1.592 ± 0.021	1.443 ± 0.010
Thickness per layer (μm)	45.9	48.2	43.7
Density (g/cm^3)	1.166 ± 0.088	1.246 ± 0.019	1.359 ± 0.049
Resin content (wt.%)	60.4 ± 4.3	27.7 ± 1.5	43.8 ± 1.4
IL concentration in epoxy (wt.%)	4	10	3
Initial cure temperature (°C)/hold time (min)	130/30	110/30	110/30

Table 2. Mechanical properties of CNTF reinforced polymer composites.

	Uni CNT roving/epoxy composite	Uni HD-CNTF/epoxy composite	Uni CNT-CoF/epoxy composite
SBS			
Strength (MPa)	34.3 ± 3.5	14.0 ± 0.9	40.3 ± 1.8
Specific strength [MPa/(g/cm^3)]	26.7 ± 2.5	11.9 ± 1.0	29.2 ± 1.2
Axial Flexure			
Strength (MPa)	214.6 ± 9.5	459.9 ± 29.4	484.0 ± 18.2
Specific strength [MPa/(g/cm^3)]	181.7 ± 8.4	375.2 ± 17.1	353.7 ± 5.1
Tangent modulus (GPa)	27.7 ± 0.4	116.2 ± 10.9	137.5 ± 3.2
Specific tangent modulus [GPa/(g/cm^3)]	23.5 ± 0.2	94.8 ± 7.1	100.5 ± 2.1
Flexural strain (%)	1.35 ± 0.42	0.56 ± 0.09	0.66 ± 0.16
Transverse Flexure			
Strength (MPa)	101.2 ± 18.3	21.1 ± 2.3	45.9 ± 5.7
Specific strength [MPa/(g/cm^3)]	80.2 ± 13.7	18.2 ± 2.0	34.4 ± 3.9
Tangent modulus (GPa)	3.2 ± 0.2	0.8 ± 0.1	1.2 ± 0.5
Specific tangent modulus [GPa/(g/cm^3)]	2.5 ± 0.1	0.7 ± 0.1	0.9 ± 0.4
Flexural strain (%)	4.28 ± 0.46	3.32 ± 0.31	4.50 ± 1.68
CLC			
Strength (MPa)	184.3 ± 21.5	231.3 ± 2.7	201.6 ± 7.3
Specific strength [MPa/(g/cm^3)]	150.3 ± 14.1	185.4 ± 0.2	146.4 ± 3.0
Young's modulus (GPa)-actuator	5.5 ± 0.9	10.7 ± 0.7	13.1 ± 2.0
Specific modulus [GPa/(g/cm^3)]-actuator	4.4 ± 0.6	8.6 ± 0.5	9.5 ± 1.6
Young's modulus (GPa)-Laser extensometer	21.3 ± 3.0	31.1 ± 8.2	34.2 ± 11.4
Specific modulus [GPa/(g/cm^3)]-Laser extensometer	17.4 ± 2.4	24.9 ± 6.3	24.7 ± 8.0
Elongation at failure-actuator (%)	5.77 ± 0.72	4.23 ± 0.18	2.57 ± 0.16
Elongation at failure-Laser extensometer (%)	2.63 ± 0.44	2.06 ± 0.75	0.90 ± 0.49
Tension			
Strength (MPa)	1059.0 ± 39.4*	3034.0 ± 345.6*	1371.9 ± 86.9
Specific strength [MPa/(g/cm^3)]	853.3 ± 27.5	2050.8 ± 187.2	1086.6 ± 70.9

Young's modulus (GPa)-actuator	54.5 ± 4.1	146.9 ± 5.1	81.7 ± 2.3
Specific modulus [GPa/(g/cm^3)]-actuator	43.9 ± 3.0	99.5 ± 3.9	64.7 ± 2.0
Young's modulus (GPa)-Laser extensometer	58.3 ± 4.8	274.1 ± 46.2	150.4 ± 21.9
Specific modulus [GPa/(g/cm^3)]-Laser extensometer	47.0 ± 4.1	193.7 ± 20.3	119.2 ± 17.7
Elongation at failure-actuator (%)	6.67 ± 1.19	3.22 ± 0.25	2.74 ± 0.41
Elongation at failure-Laser extensometer (%)	5.53 ± 1.29	1.34 ± 0.16	1.21 ± 0.17

*From reference [15].

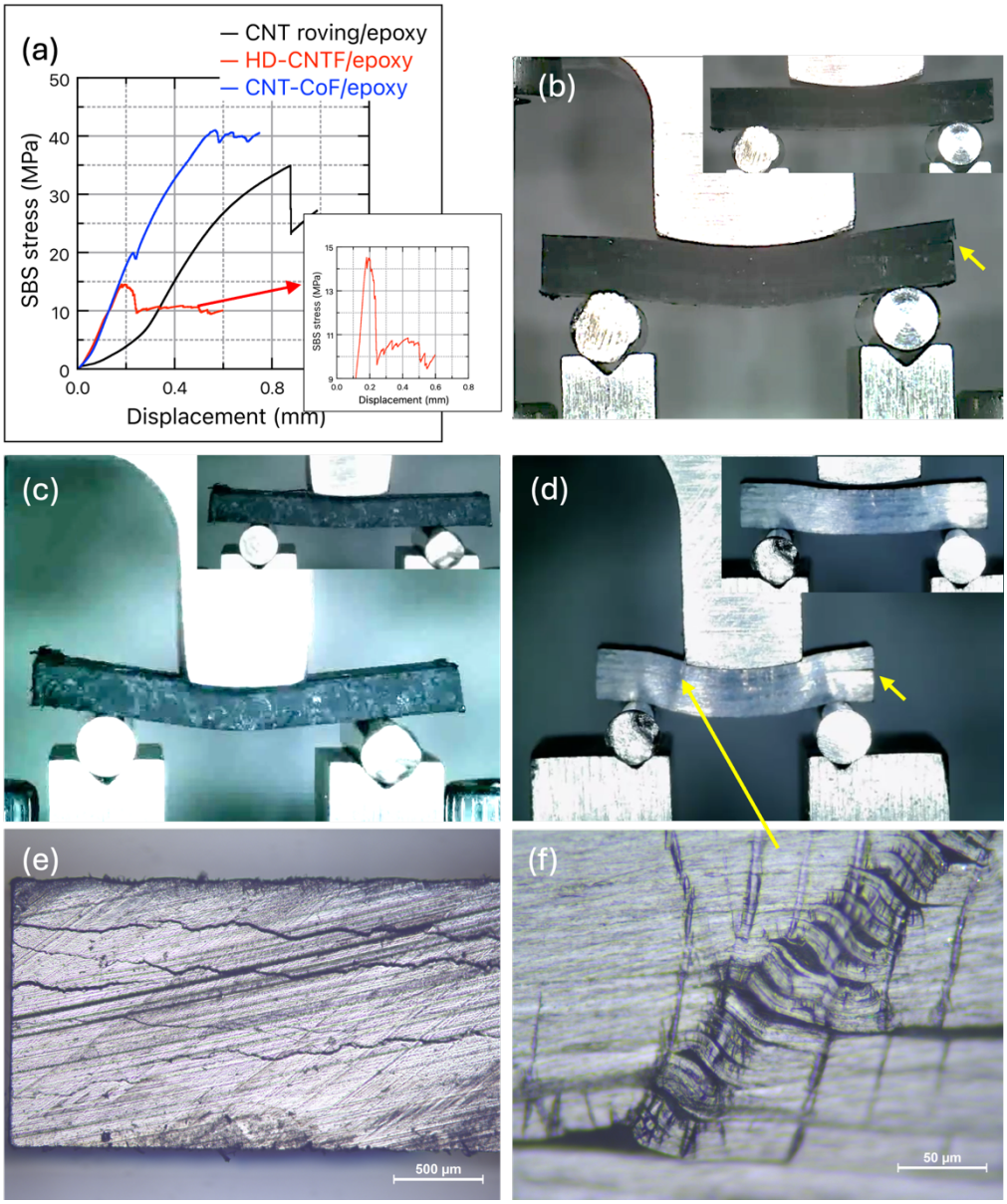


Figure 1. SBS behaviors of the CNT roving, HD-CNTF, and CNT-CoF composites. (a) Representative SBS stress vs. displacement curves of the composites. Video frames observed by portable optical microscope during the SBS tests of the (b) CNT roving, (c) HD-CNTF, and (d) CNT-CoF composites under loading before release. Insets in (b), (c), and (d) were taken after unloading the sample by returning the crosshead to the initial displacement. Post-mortem OM

images of the CNT-CoF composites were taken to provide (e) an edge-on view and (f) a cross-sectional view at a location that was highly deformed while under the load.

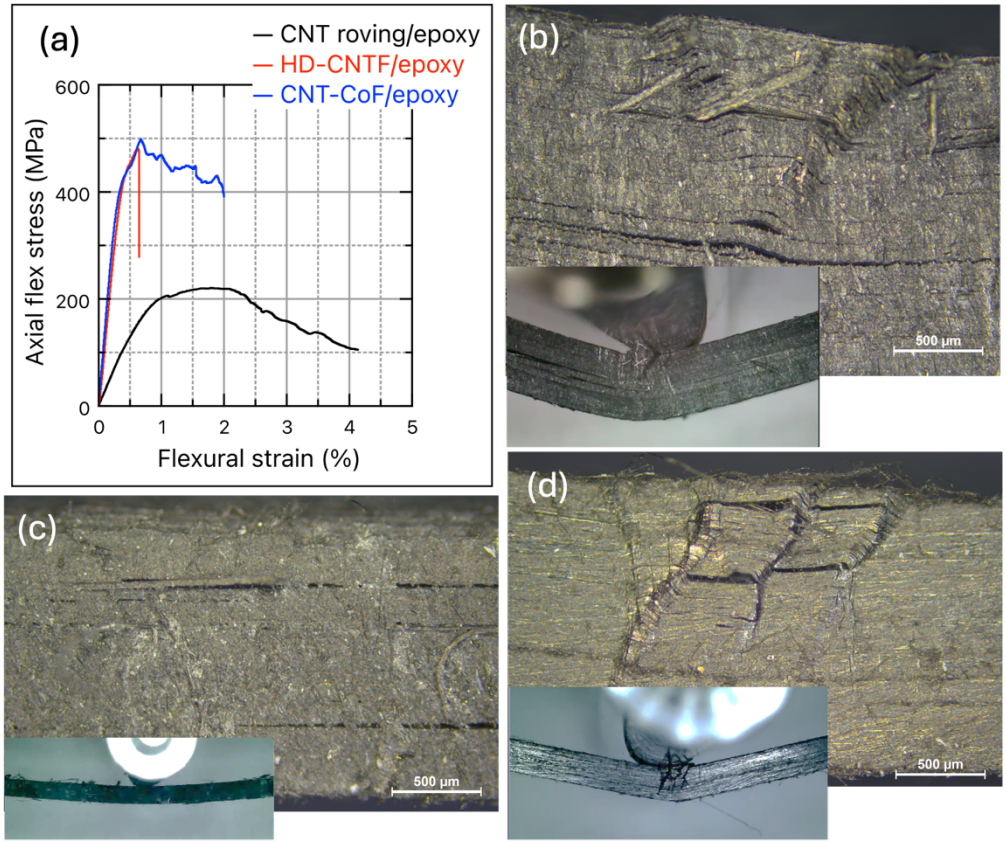


Figure 2. AF behaviors of the CNT roving, HD-CNTF, and CNT-CoF composites. (a) Representative axial flexural stress vs. strain curves of the composites. Post-mortem OM images of the (b) CNT roving, (c) HD-CNTF, and (d) CNT-CoF composites at the loading roller point after testing. Inset in each image is a video frame captured by the portable OM during the AF tests prior to release of the load.

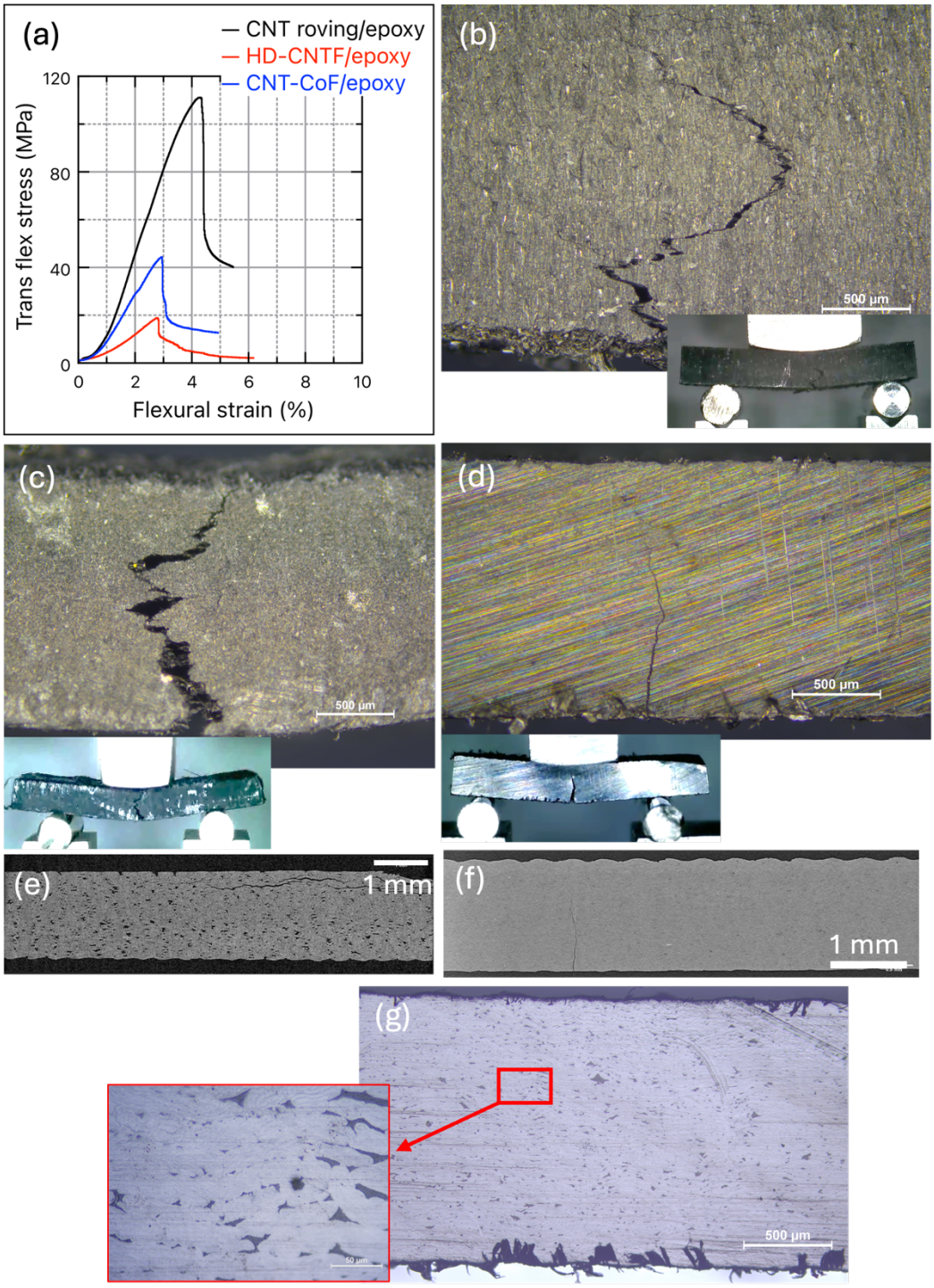


Figure 3. TF behaviors of the CNT roving, HD-CNTF, and CNT-CoF composites. (a) Representative transverse flexural stress vs. strain curves of the composites. Post-mortem OM

images of the (b) CNT roving, (c) HD-CNTF, and (d) CNT-CoF composites at the failure site after test. Insets in each image were video frames observed by portable OM during the TF tests under the loading before release. X-ray CT scan of TF specimen in the (e) HD-CNTF and (f) CNT-CoF composites. (g) OM image of TF specimen in the CNT-CoF composite before TF test. Inset is a zoom-in OM image in the certain location (red rectangle in Figure 3g).

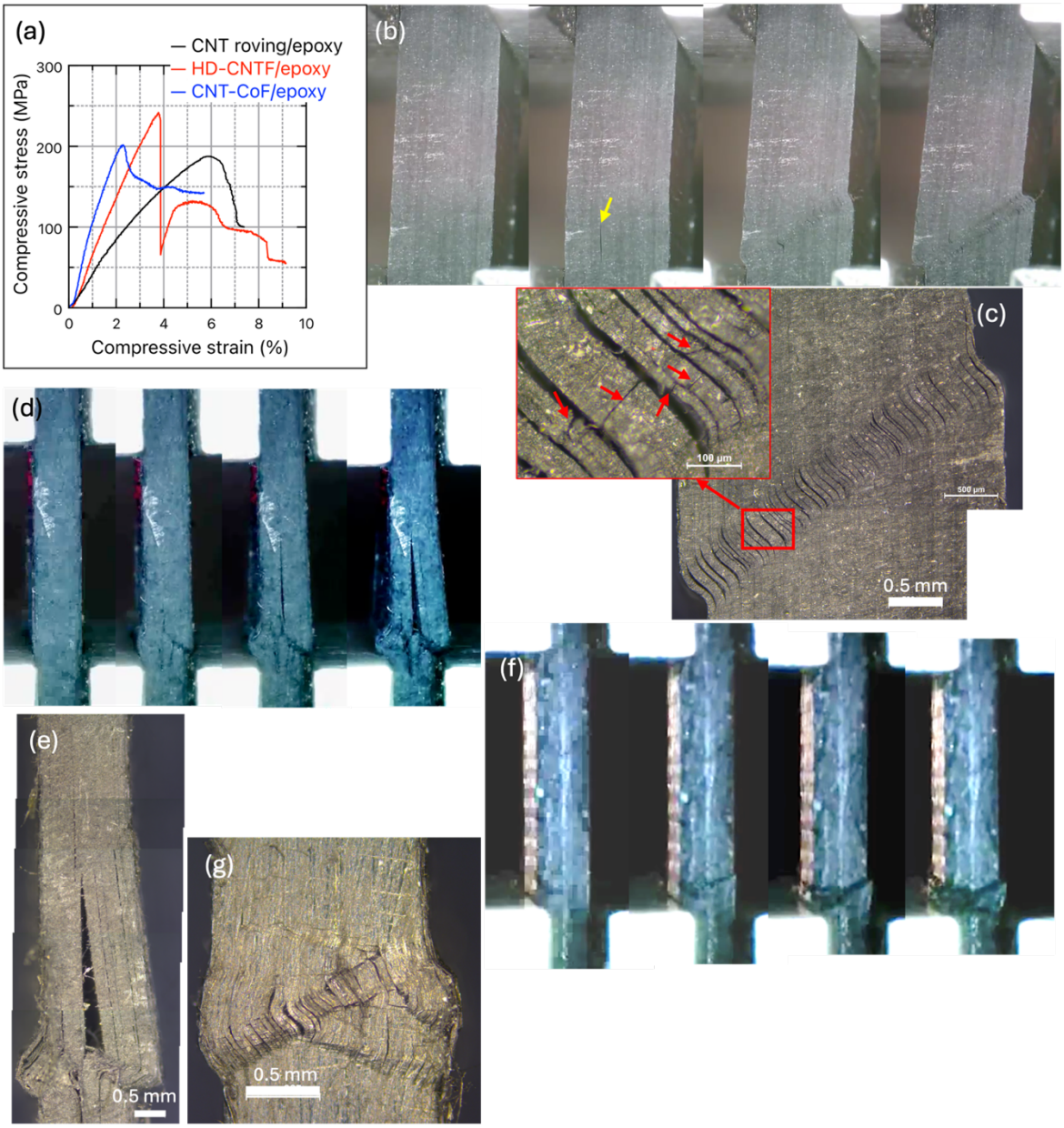


Figure 4. CLC behaviors of the CNT roving, HD-CNTF, and CNT-CoF composites. (a) Representative compressive stress vs. strain curves of the composites. Sequence of video-frame images of the (b) CNT roving, (d) HD-CNTF, and (f) CNT-CoF composites during test. Post-mortem OM images of the (c) CNT roving, (e) HD-CNTF, and (g) CNT-CoF composites after test. Inset in (c) is a zoom-in OM image showing tensile breaks at the kink band boundaries (red arrows).

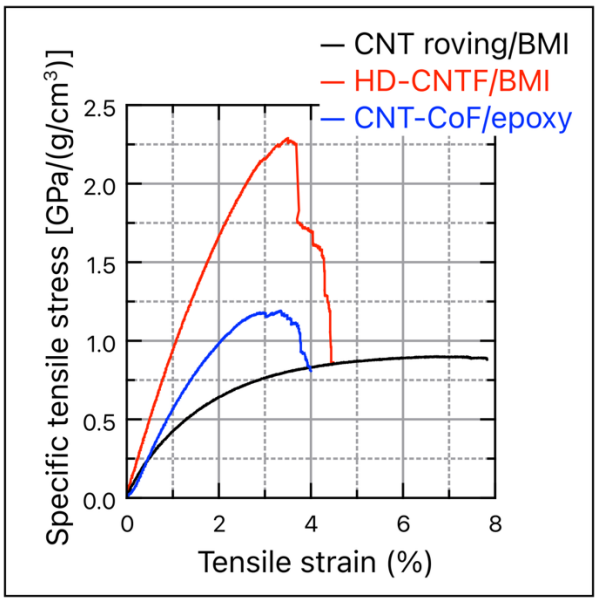


Figure 5. Representative specific tensile stress vs. strain curves of the CNT roving, HD-CNTF, and CNT-CoF composites. The data for the CNT roving and HD-CNTF composites were extracted from the reference 15 and replotted.

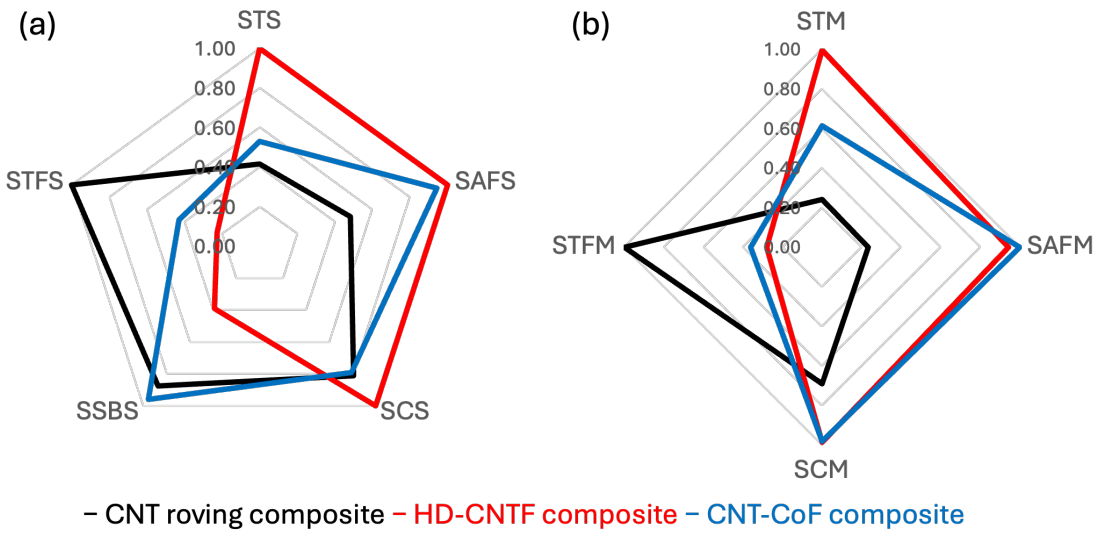


Figure 6. Radar plots of (a) specific strengths and (b) specific moduli of the CNT roving, HD-CNTF, and CNT-CoF composites under various loading conditions. Here, each acronym stands for STS (specific tensile strength), SAFS (specific axial flexural strength), SCS (specific compressive strength), SSBS (specific short beam strength), STFS (specific transverse flexural strength), STM (specific tensile modulus), SAFM (specific axial flexural modulus), SCM (specific compressive modulus), and STFM (specific trnasverse flexural modulus).

Supporting Information.

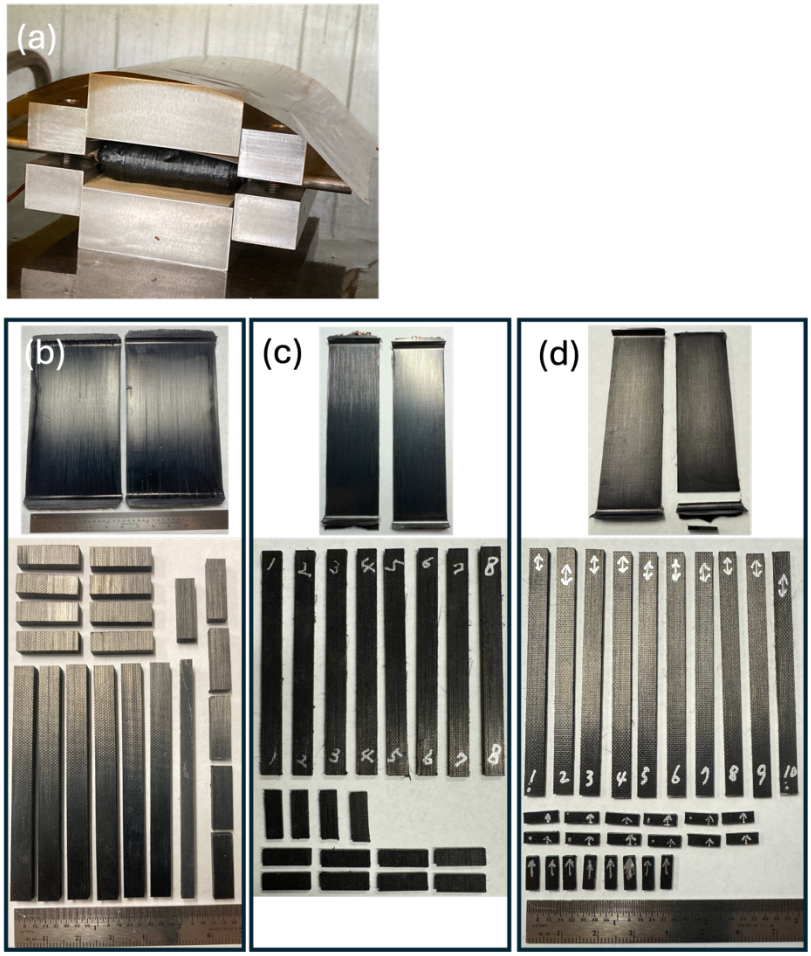


Figure S1. Digital image of (a) mold set up for hot press cure with the as-wound part sandwiched together with two plungers and two side dam blocks. Digital images of as-fabricated samples and resultant specimens of the (b) CNT roving, (c) HD-CNTF, and (d) CNT-CoF composites after cutting of curved edge to separate two coupons and cutting of specimens for multiple testing.

Dynamic rheological behavior of the EPON™ 828 and ionic liquid (IL) mixtures was measured using an Advanced Rheometric Expansion System Rheometer (Rheometrics, Inc.).

The measurements were carried out under a nitrogen atmosphere in an oscillatory shear mode using a parallel plate geometry (30 mm diameter) at a heating rate of 2.78°C/min. The top plate was oscillated at a variable strain and a fixed angular frequency of 12.5 rad/s while the lower plate was attached to a transducer that recorded the resultant torque. Approximately 0.8 mL of resin and IL (3, 7, and 10 wt.%) mixture was used per run. Storage (G') and loss (G") moduli and complex viscosity (η*) were measured as a function of time. Temperature was ramped from room temperature to 130°C and held for 30 min (Figure S2). The gel points at 130°C for the 3, 7, and 10 wt.% IL system occurred at 26.5, 12.7, and 6.5 min, respectively. The gel point can be changed by decreasing the hold temperature (i.e., 110°C) and with the incorporation of CNTs in the system.

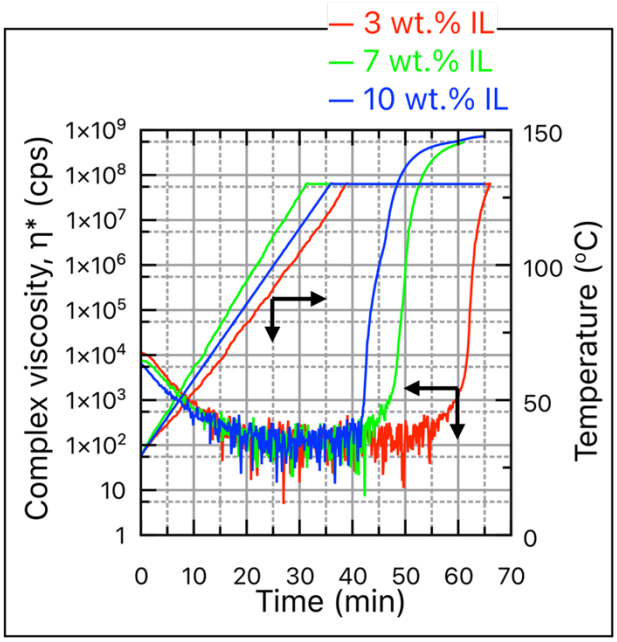


Figure S2. Rheological data with neat epoxy resin and various IL concentrations.

Neat epoxy resin specimens with 3, 5, 7, and 10 wt.% IL were fabricated using a custom-made silicone mold with proper dimensions for dog-bone shaped specimens based on ASTM D638-08

(Standard test method for tensile properties of plastics). The sample was cured by heating from room temperature to 130°C with a hold for 30 min, then ramped to 165°C with a hold for 2 hrs, and cooled to room temperature. The mechanical properties of the cured neat resin with various IL concentrations are summarized in Table S1.

Table S1. Mechanical properties of the neat epoxy resin with various IL concentrations as a cure agent.

	Neat epoxy /3 wt.% IL	Neat epoxy /5 wt.% IL	Neat epoxy /7 wt.% IL	Neat epoxy /10 wt.% IL
Tension				
Strength (MPa)	51.2 ±5.4	44.3 ± 4.3	50.8 ± 5.9	74.3 ± 8.2
Young's modulus (GPa)-Laser extensometer	2.9 ± 1.0	2.7 ± 0.6	2.9 ± 0.4	3.1 ± 0.3
Elongation at failure-Laser extensometer	2.9 ± 0.5	1.8 ± 0.3	2.1 ± 0.3	3.8 ± 1.1

Various unidirectional CNTF/epoxy composites with 3, 5, and 10 wt.% IL were fabricated and the mechanical properties of the cured composite are summarized in Table S2.

Table S2. Mechanical properties of the CNT-CoF composites.

	Uni CNT-CoF/epoxy composite (3 wt.% IL)	Uni CNT-CoF/epoxy composite (5 wt.% IL)	Uni CNT-CoF/epoxy composite (10 wt.% IL)
CNT-CoF composites			
Number of layers	33	36	34
Thickness (mm)	1.443 ± 0.010	1.968 ± 0.008	1.701 ± 0.020
Thickness per layer (μm)	43.7	54.7	50.0
Density (g/cm^3)	1.359 ± 0.049	1.337 ± 0.038	1.353 ± 0.035
Resin content (wt.%)	43.8 ± 1.4	52.2 ± 1.5	47.8 ± 1.6
SBS			
Strength (MPa)	40.3 ± 1.8	41.5 ± 4.4	36.6 ± 1.2
Specific strength [MPa/(g/cm^3)]	29.2 ± 1.2	30.5 ± 2.8	26.6 ± 0.9

Axial Flexure			
Strength (MPa)	484.0 ± 18.2	489.9 ± 28.1	494.5 ± 42.6
Specific strength [MPa/(g/cm^3)]	353.7 ± 5.1	366.9 ± 11.1	367.9 ± 18.9
Tangent modulus (GPa)	137.5 ± 3.2	119.7 ± 5.2	110.6 ± 18.4
Specific tangent modulus [GPa/(g/cm^3)]	100.5 ± 2.1	89.6 ± 1.4	82.0 ± 12.1
Flexural strain (%)	0.66 ± 0.16	0.76 ± 0.16	0.92 ± 0.22
Transverse Flexure			
Strength (MPa)	45.9 ± 5.7	44.0 ± 2.2	45.3 ± 4.6
Specific strength [MPa/(g/cm^3)]	34.4 ± 3.9	32.9 ± 2.0	33.6 ± 3.2
Tangent modulus (GPa)	1.2 ± 0.5	1.4 ± 0.1	1.0 ± 0.1
Specific tangent modulus [GPa/(g/cm^3)]	0.9 ± 0.4	1.1 ± 0.1	0.8 ± 0.1
Flexural strain (%)	4.50 ± 1.68	4.43 ± 0.23	7.31 ± 1.29
CLC			
Strength (MPa)	201.6 ± 7.3	233.7 ± 10.1	196.2 ± 7.0
Specific strength [MPa/(g/cm^3)]	146.4 ± 3.0	173.6 ± 3.3	144.3 ± 3.6
Young's modulus (GPa)-actuator	13.1 ± 2.0	9.5 ± 1.1	10.5 ± 2.0
Specific modulus [GPa/(g/cm^3)]-actuator	9.5 ± 1.6	7.1 ± 0.8	7.7 ± 1.6
Young's modulus (GPa)-Laser extensometer	34.2 ± 11.4	33.9 ± 4.6	33.9 ± 7.8
Specific modulus [GPa/(g/cm^3)]-Laser extensometer	24.7 ± 8.0	25.2 ± 3.9	25.0 ± 6.0
Elongation at failure-actuator	2.57 ± 0.16	4.43 ± 0.57	3.27 ± 0.33
Elongation at failure-Laser extensometer	0.90 ± 0.49	1.45 ± 0.18	0.98 ± 0.28